94 KSME Journal, Vol. 8, No. 1, pp. 94~102, 1994

Interpretation of Emission Image of an Axisymmetric Diffusion Flame into 2-Dimensional Temperature Data Using a Simplified Computed Tomography

Kwangsoon Ha* and Sangmin Choi*

(Received August 23, 1993)

Photographic images of axisymmetric diffusion flames were interpreted using the computed tomographic techinque. The two dimensional images of an axisymmetric diffusion flame were measured by a commercial CCD array camera and a frame grabber. The image data were then used to reconstruct the original three dimensional spatially resolved distributions of emission intensities by using the computed tomographic technique. The reconstructed volumetric emission intensities were then converted into optical temperatures of soot particles by assuming that the system response parameters were constant. The constants were determined from the calibration tests with a blackbody cavity, and with thermocouple measurements. The reconstructed temperatures, which were considered as the temperatures of soot particles, showed reasonable resemblance to the expected temperature distribution. The characteristics of the optical system, such as F number and pixel distance (magnification of image), with respect to the accuracy of reconstructed data were discussed.

Key Words: Computed Tomography(CT), Emission Image, Axisymmetric Diffusion Flame, CCD Camera

1. Introduction

Spatially resolved measurement of flame temperature is of great importance in combustion studies. Thermocouple probes have been widely used for temperature measurements, but problems remain associated with this technique such as measurement erros caused by temporal fluctuation, catalytic reaction, and radiative losses of the probe. Nonintrusive methods, such as spectroscopic band methods (Brewer, L.E. et al., 1972), monochromatic line of sight transmission methods coupled with tomography (Santoro, R. J. et al., 1983), coherent anti-Stokes Raman spectroscopy (CARS) (Boedeker, L.R. et al., 1987), and planar laser-induced fluorescene(Lee, M. P. et al., 1986) have been suggested to determine the spatial distribution of species concentrations and temperatures in the flames. Each method has its own set of assumptions, limitations, and strengths.

Computed tomography(CT) is a noncontact measurement technique which has been widely used in medical diagnosis. Using this technique, one can reconstruct any 2-D physical distribution of arbitrary tomographic layer in an object. The principle of this technique is straightforward and can be applied not only with X-ray but also with γ-ray, ultrasound, and nuclear magnetic resonance. Infrared emission(Uchiyama, H. et al., 1985) and sound wave have been also used to obtain 3-D temperature distribution in flames.

However, for mathematical reconstruction of two dimensional images by CT technique, many line-of-sight measurements across the object are required. These measurements are tedious and include errors caused by fluctuation of the flame and misalignment of the optical system. In ordser to circumvent these disadvantages of CT, we

* Department of Mechanical Engineering Korea Advanced Institute of Science and Technology

present a simple computed tomography using a commercial CCD array. CCD array camera with image processing technique has been previously employed to visualize the reaction zone of a flame, in which the light emission images of radicals (OH and CH) were visualized by processing the monochromatic images of the flame at and in the neighborhood of the emission band of the radicals (Mizutani, Y. et al., 1988).

Our observation is made using a typical coannular laminar diffusion flame under atmospheric pressure condition. The temperature of sooting laminar diffusion flame is an important controlling variable for soot formation. However, temperature is difficult to measure with a thermocouple in a sooting environment because of the soot deposition and growth on the probe surface, and the subsequent radiative loss. That is why thermocouple temperatures are often interpreted as a qualitative indicator. Nonintrusive methods, such as CARS and FT-R (Best P.E., et al., 1991), have been introduced to find the temperatures in sooting laminar diffusion flames.

In this paper, spatially resolved temperature distributions in a sooting axisymmetric laminar diffusion flame are qualitatively obtained by simple computed tomography using a commercial CCD array camera. Data flow in this paper is shown in Fig. 1. Commercial CCD array can be used to obtain 2-D line-of-sight data like a method of taking a photograph. Single-shot image obtained by CCD array is converted into 3-D point intensity by CT algorithm. The method of calculating temperature from point intensity is exracted from blackbody source data. Characteristics of the image system, such as F number and pixel distance (magnification of image) are discussed with respect to the accurary of reconstructed data.

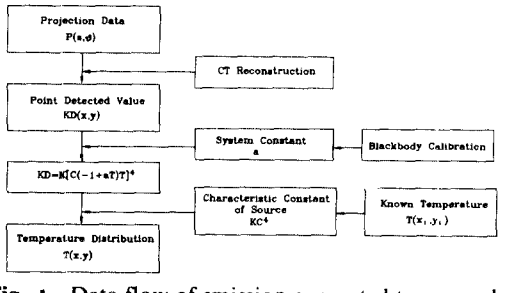

Fig. 1 Data flow of emission computed tomography

2. Theory of Emission Computed Tomography

2.1 The Reconstruction Algorithm

Let us assume that the intensity distribution in an arbitary transaxial layer in the flame is $\varepsilon_\lambda I_{b\lambda}(x, y)$ which represents the radiation from a graybody. As shown in Fig. 2, the detected value $P(s,\theta)$ is a projection data which is expressed by the line integral,

$$P(s,\theta)=\int_L\int_\lambda S_\lambda \kappa_\lambda \varepsilon_\lambda I_{b\lambda} \exp\left\{-\int_{L'}\kappa_\lambda(x',\, y')\, dL'\right\} d\lambda dL \qquad (1)$$

where S_λ : the wavelength sensitivity of the detector

ε_λ : spectral emissivity

$K_\lambda(x, y)$: the absorption coefficient

L : the path length from the detector surface to the far edge of the flame

L' : the path length from the detector surface to the point(x',y')

By defining a rotated coordinate (s,θ) system,

$$\begin{cases} s=x\cos\theta+y\sin\theta \\ t=-x\sin\theta+y\cos\theta \end{cases} \qquad (2)$$

Assuming that $\kappa_\lambda(x,y)$ is a small constant value

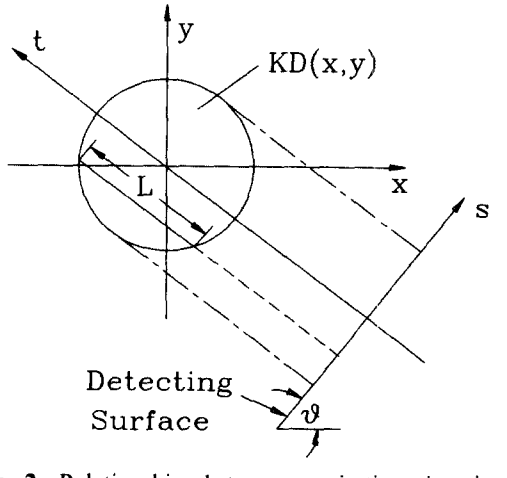

Fig. 2 Relationship between projection imaging geometry in CT scanning

and independent of temperature and pressure in a local region, Eq.(1) is simplified to

$$P(s,\theta)=\int_L\int_\lambda KS_\lambda I_{b\lambda}(x,y)d\lambda\, dL \qquad (3)$$

$$\int_L K\, D(x,y)\, dL$$

where $K=\varepsilon_\lambda k_\lambda \exp\left\{-\int_L' k_\lambda(x',y')\, dL'\right\}$

$$D(x,y)=\int_\lambda S_\lambda I_{b\lambda}(x,y)\, d\lambda$$

Therefore, $P(s,\theta)$ is the projection of $KD(x,y)$ at an alngle θ which corresponds to a line integral for the path distance of L. The reconstruction problem is to invert a finite number of equations in the form od Eq.(3) for different values of θ to yield an estimate of $KD(x,y)$.

Further assuming that no other intensity source than the flame is present in the optical path, Eq. (3) is extended to.

$$P(s,\theta)=\int_{-\infty}^{+\infty} KD(x,y)\, dt \qquad (4)$$

By the projection-slice theorem, the one dimensional Fourier transform with respect to s of the projection $P(s,\theta)$ is equal to the cental slice, at angle θ, of the two dimensional Fourier transform of the object $KD(x,y)$. Therefore $KD(x,y)$ can be obtained by the two dimensional inverse Fourier transform of the result which is one dimensional Fourier transform of $P(s,\theta)$. The convolution theorem was used to perform the two-dimensional inverse Fourier transformation, and the following equation is derived.

$$KD(x,y)=\frac{1}{2\pi}\int_0^\pi\int_{-\infty}^{+\infty} P(s,\theta))\cdot\phi(x\cos\theta + y\sin\theta - s)\, ds\, d\theta \qquad (5)$$

Discretizing Eq.(5), we obtain

$$KD(x,y)=\frac{a}{2N}\sum_{j=1}^{N}\sum_{k=1}^{M} P(s_k,\theta_j)\cdot\phi(x\cos\theta_j + y\sin\theta_j - s_k) \qquad (6)$$

where $\theta_j=\frac{(j-1)\pi}{N}$, $s_k=ka$,

N is the number of projections, and M is the number of measured data along one projection angle. Generally, the alrger the value of M and N, the more enhanced is the reconstructed image (Dudgeon, D.E. et al., 1984; Jain, A.K., 1989).

ϕ is called projection filter. Ideally, this filter has the frequency response $|\omega|$. Since the filter gain increases with frequency, high-frequency noise will be amplified. Thus the filter must be chosen to minimize the deterioration. The modified Shepp-Logan filter (Kwon, Y.S. et al., 1977) was chosen as follows.

$$\bar{\phi}(s_k)=0.4\phi(s_k)+0.3\phi(s_{k+1})+0.3\phi(s_{k-1})$$

$$\phi(s_k)=\frac{-4}{\pi a^2(4k^2-1)} \qquad (7)$$

2.2 Calculation of Temperature

Total emissive power of a graybody source is proportional to T^4 according to the Stefan-Boltzmann law. However, visible image detectors have a limited bandwith of response and spectral responsivities are not constant. Preliminary investigation have led us to propose and empirical relation of the detected power to the temperatures of the object in the form of $[(-1+aT)T]^4$. In such cases, the local radiative emissive power can be related with the local temperature as Eq. (8).

$$KD(x,y)=K[C(-1+aT)T]^4 \qquad (8)$$

where a is system response constant, and C is a constant of object properties such as emissivity.

A balckbody furnace was used to obtain the value of the constant a. The blackbody cavity was made of stainless steel and had a cylindrical hole of 11 mm diameter and 80 mm depth. Emission

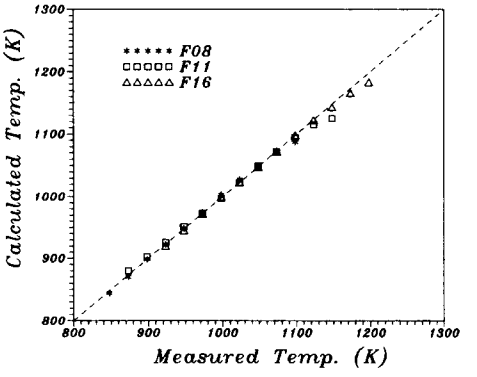

Fig. 3 Verification of constant value a by blackbody calibration [F number is the ratio of the effective focal length to the clear aperture of the Nikon standard lens (NIKKOR F1. 4, 50 mm)]

from the blackbody hole was captured by CCD camera. The 17×17 pixel mean value was considered as $D(x,y)$. Constant value of a was chosen to be 0.166 K^{-1} for which Eq.(8) excellently agrees with the blackbody temperature measured by thermocouple (Fig.3).

In order to interpret the spatially resolved radiative power in terms of temperature distribution, temperature at one point (x_1,y_1) must be known. The constant KC^4 can be found with the know temperature, and then the reconstructed value of $KD(x,y)$ is converted into the local temperature.

3. Experimental Apparatus

A schematic of experimental setup to capture the flame image is shown in Fig. 4. The projection data from flame was captured with a CCD array camera and converted into numerical forms by an image processor and then stored in a personal computer. A commercial CCD array camera (SEN TECH Co. STC-10J) with a Nikon standard lens(NIKKOR F1.4, 50 mm) was used. An image processor (MVP-AT) was used to grab flame images and to store as a set of horizontal grid of small regions containing picture elements. The frame grabber had 8-bit resolution, translated into a gray level from 0 to 255. The distance between the flame and the imaging camera was adjusted, and the magnification of image (it is equivalent to the number of pixels which represent the flame.) was determined. The real distance in the flame corresponding to pixel to pixel (hereinafter, this called as pixel distance) was also varied, and the captured flame image was magnified or reduced, accordingly.

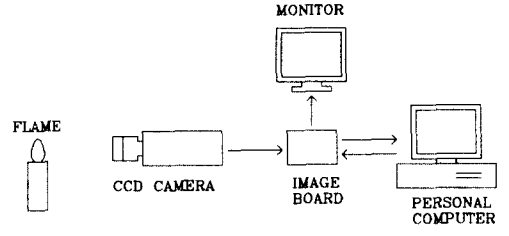

Fig. 4 Schematic of experimental setup for capturing flame image

Observation was made using a typical coannular laminar diffusion flame under atmospheric pressure conditions. This burner flame has been the subject of previous investigation, where soot particle measurements were studied (Santoro, R.J. et al., 1983). The burner consisted of one concentric brass tube of 15 mm in diameter and an acryl tube of 120 mm inner diameter with propane flowing through the central brass tube and air through the outer annulus. The fuel passage contained iron screens (70 mesh) and 3.0 mm glass beads to provide a uniform exit flow profile. The air passage was also filled with a series of iron screens (40 mesh) and 3.0 mm glass beads. Visible region of the flame is extended to about 120 mm.

4. Results

4.1 The Verifications of Reconstruction Program

The reconstruction program was verified for the axisymmetric step function $[z=f(r)]$ as Eq. (9).

$$\begin{cases} z=1, & r^2=x^2+y^2 \leqq 1.0 \\ z=0, & r^2=x^2+y^2 > 1.0 \end{cases} \tag{9}$$

The comparision of reconstructed values to the step function is shown in Fig. 5. The reconstruction was in good agreement within the error range of 0.614 percent from $r=0$ to $r=0.9$. It is usually expected that the higher accuracy of reconstruc-

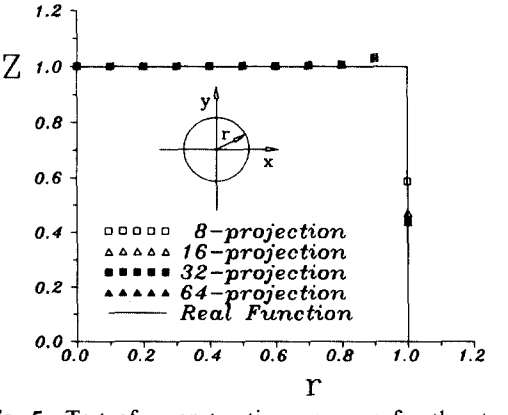

Fig. 5 Test of reconstruction program for the step function

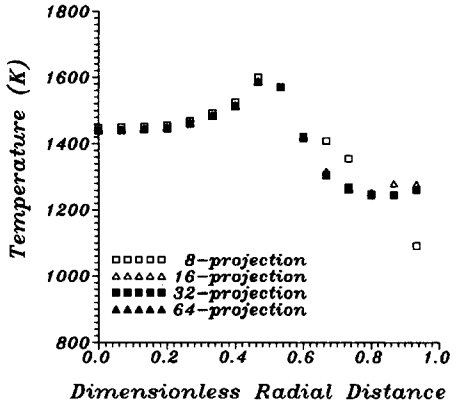

Fig. 6 Test of reconstruction program for the experimental Data

tion can be achieved with higher number of projections, N (in Eq.(6)). However, in this case, the accuracy of 8 projections was almost same as that of 16 projections.

Fig. 6 represents the variations of accuracies of the reconstructed values for the experimental data with four cases of the number of projections. According to this figure, as there is no improvement in accuracy for the cases of finer than 32 projections, 32-projection was chosen for further calculation.

4.2 Reconstructed Temperature Distribution

To find spatially resolved temperature, known temperature was selected as 1571 K at $r=0.6$, $X=0.32$ from the thermocouple (Pt-Pt13%Rh) measurement (r is the dimensionless radial distance, that is, $r=0$ at the burner center and $r=1$ at the burner rim, and X is the dimensionless height, that is, $X=0$ at the burner lip and $X=1$ at the top of the visible flame region.). The contour diagrams of reconstructed temperatures are shown in Fig. 7.

The uncertainty of reconstructed temperature was evaluated according to the procedure of Moffat (Moffat, R.J., 1988). Error sources included in the reconstructed temperature could be classified into two parts. One was associated with the experiment of flame grabbing and calculation of temperature from point detected value. The error of flame grabbing experiment was due to the

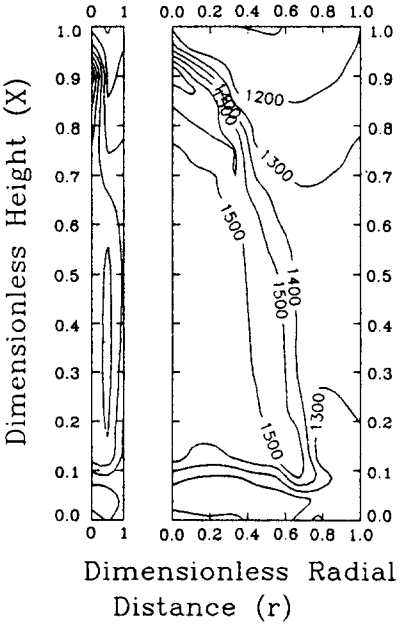

Fig. 7 Contour plots of recunstruction temperatures (0.294 mm/pixel, F11) [The left figure is drawn with a true aspect ratio of 7.5 to 120, while the aspect ratio of the right side figure is 7.5 to 20 for easier observation]

non-uniformity, non-linearity, signal-to-noise ratio, and responsivity of CCD array. And the error of Eq.(8) was that of the calculation of temperature from the point detected value. This first part was evaluated from the calibration experiment with a blackbody cavity. The other part which affected the uncertainty of the reconstructed temperature was associated with the reconstruction program. This part was obtained by considering the step function of Eq.(9): Consequently, the reconstructed temperature had the uncertainty level from 1.51% minimum to 1.87% maximum. This uncertainty did not include the factors generated by the object, such as flame flicker and non-ideal symmetry of the flame. We only evaluated the uncertainty of our scheme.

4.2.1 Radial temperature distribution.

Radial temperature profiles for four F numbers of CCD camera are plotted in Fig. 8. Figures 8(a), 8(b), 8(c), and 8(d) represent the dimensionless heights above burner lip $X=0.32$, 0.416, 0.56, and 0.80 respectively. As the equivalent image

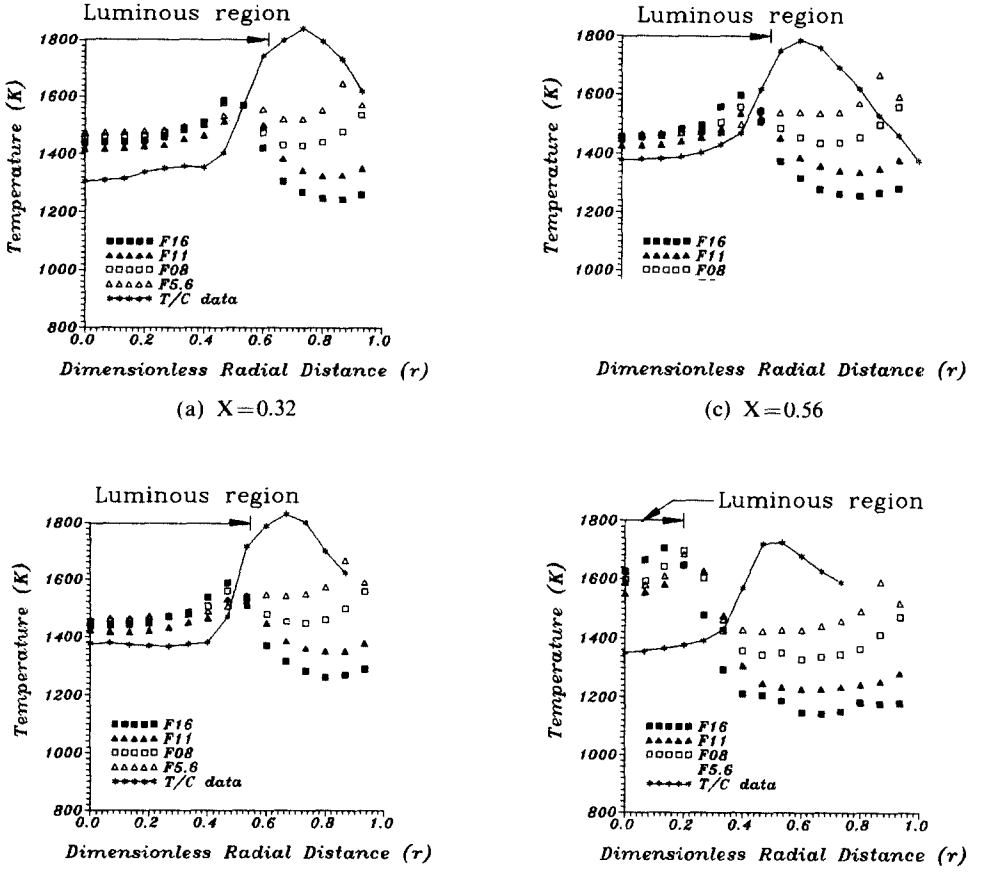

Fig. 8 Reconstruction temperatures across a diameter for F number (0.294 mm/pixel)

distance per each pixel is 0.294 mm/pixel, the error of height is 0.147 mm. The edges of the luminous envelop are measured to be $r=0.61$ at $X=0.32$, $r=0.55$ at $X=0.416$, $r=0.49$ at $X=0.56$, and $r=0.2$ at $X=0.80$ by PMT power output. Calculated temperatures represent maximum values at edges of luminous regions, while thermocouple temperatures show maximum at slightly outer regions. The flame diameter is believed to decrease for the higher axial distance because the calculated flame temperature is maximum at the visible boundary in this case. The reasons for the discrepancy in luminous region include the presence of soot adhered to the thermocouple bead, and the subsequent radiative losses. The scattering of calculated temperature in the outside of the luminous region is caused by background noise and optical distortion. As the reconstructed temperatures are calculated from soot emission, calculated temperatures are only useful in the sooting area.

4.2.2 F number.

The results of calcualted temperatures are independent of the variations of F number. As the F number decreases, the intensity on CCD array increase, the image becomes blur, and CCD array is more likely to be saturated. So, it is possible to generate the errors due to blurred image, and the saturation of CCD array elements.

4.2.3 Temperature profile along the center line.

Temperatures along the center line of flame for four F numbers of CCD caemra are plotted in Fig. 9 as a function of dimensionless height X.

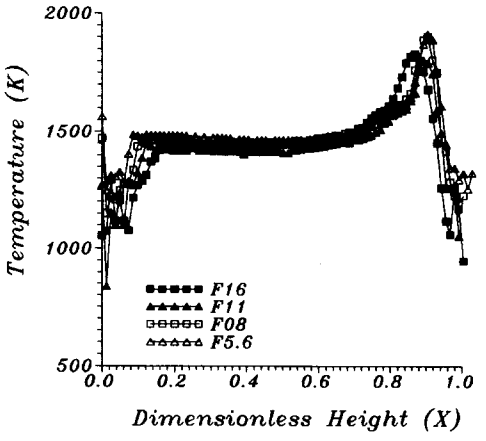

Fig. 9 Temperature profiles along the center line of the flame (0.294 mm/pixel)

The general behavior is shown; temperature rapidly increases near the bottom of the flame, stays almost constant at the central region, and increases again near the top of the flame. The large error of calculated temperature on the bottom region of the flame is due to the variations of flame parameters, such as absorption coefficient and flame emissivity. In fact, the region is optically clear with no sign of apparent soot presence.

4.2.4 Symmetry.

As the flame is assumed to be axisymmetric, only a half part of flame image is used to reconstruct spatially resolved intensity distribution. So, the left and right half part of flame image are separated, and the temperature distributions are reconstructed with each half part. In Fig. 10, the symmetry of the flame temperature is justified.

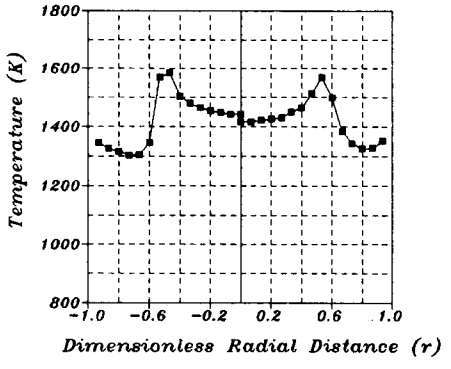

(a) X=0.32

Because the know reference temperature (1571 K at $r=0.6$, $X=0.32$) is applied to each part seprarately, the left and right reconstructed value at $r=0$ are not same. Deviation from symmetry is

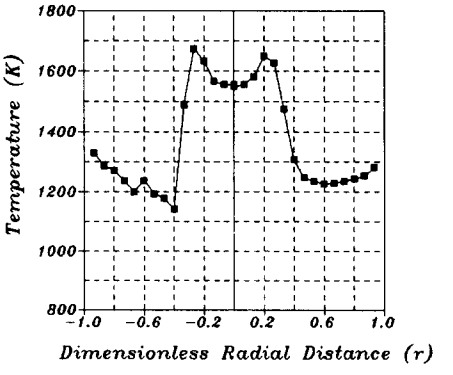

(b) X=0.416

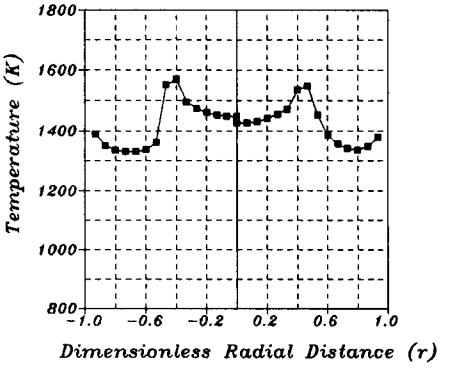

(c) X=0.56

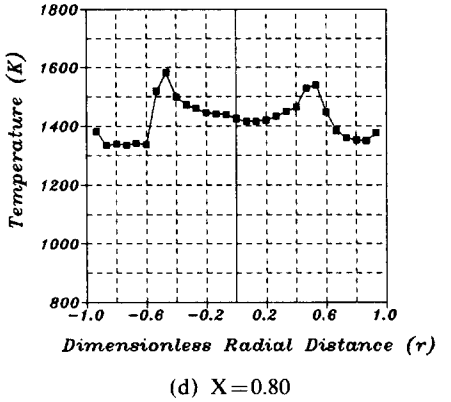

(d) X=0.80

Fig. 10 Verification of symmetry of temperature distribution (0.294 mm/pixel, F11)

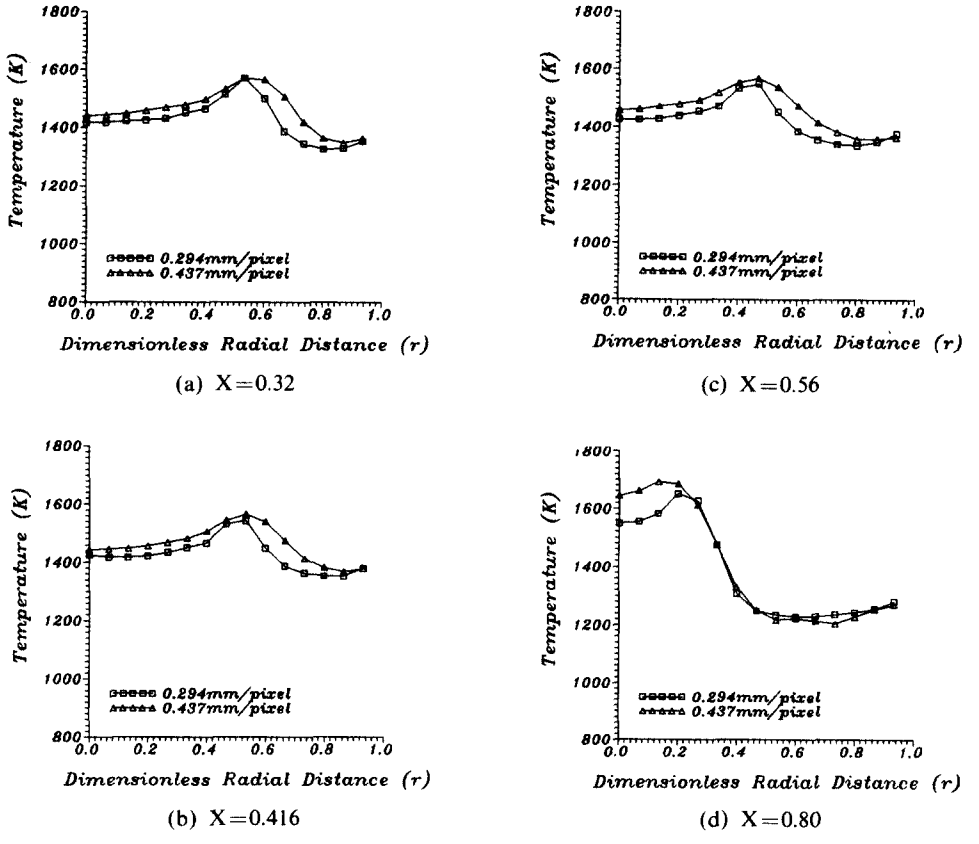

Fig. 11 Effect of variation in pixel distance (F11)

believed to be related with the nonuniformity of detectors, non-ideal symmetry of the flame, and inaccurary in determining the center line.

4.2.5 Pixel distance (magnification of image). The effect of the variation in pixel distance (magnification of image) is shown in Fig. 11. The number of pixel stored in computer was about 50 in radial direction and 415 along the height in case of 0.294 mm/pixel,and 35 in radial drection and 285 along the height in case of 0.437 mm/pixel. At the larger pixel distance, the larger error is expected because of the smaller number of measured data. However, in this case, the effect is small.

5. Conclusions

Photographic images of axisymmetric diffusion flames were interpreted using the computed tomographic technique, and a method of interpreting the intensity distribution in terms of temperature was suggested. Reconstructed temperatures, considered to be the temperatures of soot particles, showed reasonable resemblance to the expected temeprature distribution. Characteristics of the optical system, such as F number and pixel distance of CCD array camera, were found to be insignificant on the accuracy of 3-D reconstructed data. This technique can be easily applied to the problems which depend on time. If an object is axisymmetric, only single-shot image is required to obtain 3-D temperature distributions. Therefore, the scheme can be applied to the qualitative studies of transient and turbulent combustion phenomena. And, as the reconstruction results are almost independent of the optical system parameters-F number and magnification of image-, this scheme can be satisfactorily used in practical

application.

However, some of limitation of this method still remain: the reconstructed temperatures are not free from the inherent errors in finding the known temeprature because only the relative temperatures are calculated, and a calibration to a known temperature is required; commercial CCD array cameras have relatively low detectivity and poor linearity; the interpretation of temperature from the soot emission is only empirical. However, it is expected that these limitations can be overcome by using soot emissivity data, two-color pyrometries, and high performance image detectors.

References

Best, P. E., Chien, P. L., Carangelo, R. M and Solomon, P. R., 1991, "Tomographic Reconstruction of FT-IR Emission and Transmission Spectra in a Sooting Laminar Diffusioin Flame: Species Concentrations and Temperatures," *Combust. & Flame,* Vol. 85, pp. 309~318.

Boedeker, L. R. and Dobbs, G. M., 1986, "CARS Temperature Measurements in Sooting, Laminar Diffusion Flames," *Combust. Sci. & Tech.*, Vol. 46, pp. 310~323.

Brewer, L. E. and Limbaugh, C. C., 1972, "Infrared Band Model Technique for Combustion Diagnostics," *Appl. Opt.*, Vol. 11, No. 5, pp. 1200~1204.

Dudgeon, D. E. and Mersereau, R. M., 1984, "Multidimensional Digital Signal Processing," pp. 363~390, Prentice-Hall, Inc.

Hertz, H. M and Faris, G. W., 1988, "Emission Tomography of Flame Radicals," *Opt. Lett.,* Vol. 13, No. 5, pp. 351~353.

Jain, A. K., 1989, *Fundamentals of Digital Image Processing,*, pp. 431~475, Prentice-Hall International, Inc.

Kwon, Y. S., Reed I. S. and Truong, T. K., 1977, "A GEneralized |w|-Filter for 3-D Reconstruction," *IEEE Trans. on Nuclear Sci.,* Vol. NS-24, No. 5, pp. 1990~1998.

Lee, M. P., Paul, P.H. and Hanson, R. K. 1986, "Laser-Fluorescence Imaging of O_2 in Combustion Flows using an ArF Laser," *Opt. Lett.*, Vol. 11, No. 1, pp. 7~9.

Lee, M. P., Paul, P. H. and Hanson, R. K., 1987, "Quantative Imaging of Temperature Fields in Air using Planar Laser-Induced Fluorescence of O_2," Opt. Lett., Vol. 12, No. 2, pp. 75~77.

Mizutani, Y., Saeki, T. and Nakabe, K., 1988, "Visualization of the Reaction Zone of a Flame by Image Processing (Further Report)," *J. of JSME*, Vol. 54, No. 504, pp. 2219~2227.

Moffat, R. J., 1988, "Describing the Uncertainties in Experimental Results," *Experimental Thermal and Fluid Science*, Vol. 1, p. 3~17.

Santoro, R. J., Semerjian, H. G. and Dobbins R. A., 1983, "Soot Paticle Measurements in Diffusion Flames," *Combust. & Flame*, Vol. 51, pp. 203~218.

Uchiyama, H., Nakajima, M. and Yuta, S., 1985, "Measurement of Flame Temperature Distribution by IR Emission computed Tomography," *Appl. Opt.*, Vol. 24, No. 23, pp. 4111~4116.